doi.org/10.1002/hlca.202400155

RESEARCH ARTICLE

HELVETICA chimica acta

Single Molecule Conductance of Anthraquinone-Based Molecular Wire: Effect of the Anchoring Group

František Vavrek,[a] Jindřich Gasior,[a] Jakub Šebera,[a] Michal Valášek,[b] Gábor Mészáros,[c] and Magdaléna Hromadová*[a]

[a] Department of Electrochemistry at the Nanoscale, J. Heyrovský Institute of Physical Chemistry of the Czech Academy of Sciences, Dolejškova 3, 182 00 Prague 8, Czech Republic, e-mail: magdalena.hromadova@jh-inst.cas.cz

[b] Institute of Nanotechnology, Karlsruhe Institute of Technology, P.O. Box 3640, 76021 Karlsruhe, Germany

[c] Institute of Materials and Environmental Chemistry, HUN-REN Research Centre for Natural Sciences, Magyar tudósok körútja 2, 1117 Budapest, Hungary

Dedicated to Prof. *Marcel Mayor* on the occasion of his 60th birthday

Functional molecular electronics require molecular design that provides integrity and stability. In this work, we explored two types of single molecule devices differing in anchoring to the conducting leads. Single molecule conductance was measured by STM break junction method and the molecular conductor was composed of the redox active anthraquinone center (switching element) containing either 4-pyridyl or *p*-phenylene thioacetate anchoring groups. The experimental results were supported by quantum chemical charge transport calculations. Molecular junctions containing 4-pyridyl anchors displayed two stable configurations with conductance values of 4.9 nS and 20 pS, respectively. Molecules anchored via *p*-phenylene thioacetate groups led to one main junction configuration with conductance of 0.1 nS. Junctions employing 4-pyridyl anchoring groups had higher junction formation probability, which in combination with lower conductance makes them better candidates for switching purposes.

Keywords: molecular electronics, STM break junction, anthraquinone, anchoring group, DFT/NEGF calculations.

Introduction

Signal switching is one of the key elements in the design of functional nanoscale molecular electronics systems. For this reason, there is a constant demand for new molecules that can be reversibly switched between two or more (meta)stable states with the help of external stimuli.[1,2]

Molecular switches can be divided into two main groups: *conformational* and *redox active* switches. In the *conformational* switch the conductance G changes either due to molecular reorientation or due to the ability of molecule to be in several (at least two) stable isomeric states upon external stimuli. The change of conductance in *redox active* switches is related to electrochemical redox reactions that take place in the device.[2] External stimuli for switching between individual states include light, temperature, chemical (*e.g.* acid-base interactions) as well as electrochemical processes.[3–16] Thanks to these numerous possibilities to control the switching of the molecular conductance, the potential of molecular switches is not limited to the function implied by their name, but under appropriately chosen conditions, selected systems can also act as molecular transistors[13,17] or memristors.[18,19]

Conductance of a single molecule device is often influenced by the choice of the anchoring

Supporting information for this article is available on the WWW under https://doi.org/10.1002/hlca.202400155

groups.[9,20–33] Different anchoring groups have different affinity towards the electrode surface and determine the type of charge transporting orbital in a single molecule junction. The pronounced effect of anchoring groups on the charge transport efficiency has been demonstrated, when the change of the contact groups from electron-deficient 4-pyridyl to electron-rich 4-thioanisole inverted the trend of conductance in a series of molecular wires.[29] Multipodal anchoring enables better control over the MJ configuration and conductance.[34–40] The anchoring groups themselves can serve as switching elements.[41] Recently, the effect of anchoring groups was studied as part of the molecular switch design.[42,43]

In this work, we study the effect of anchoring groups on the conductance properties of a *redox-active* switch based on the anthraquinone/anthracene-9,10-diol redox couple, which is considered to be one of the most promising systems for signal switching.[44–46] We focus on the anthraquinone part of the couple, which for the purpose of switching should display the lowest conductance value.

Figure 1 shows the chemical structure of molecules **AQ-1** and **AQ-2** used in this manuscript. Both studied molecules contain an identical anthraquinone center, which is connected via a conducting ethynylene linker in positions 2 and 6 to either 4-pyridyl (molecule **AQ-1**) or phenylene thioacetate (molecule **AQ-2**) anchoring groups. They should affect the mode of charge transport in a following way. Based on previous results, 4-pyridyl should promote charge transport via LUMO orbital of the MJ system, whereas HOMO should be the main charge transporting orbital in the case of thiol anchoring after the cleavage of the protecting acetate groups.[9] In addition to these differences the choice of anchoring groups should impact the MJ formation probability and stability, the energy of the frontier orbitals, and the spin state of the charge carriers.[2]

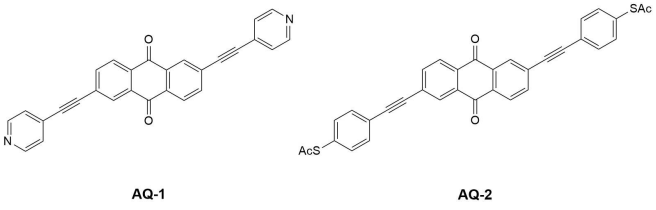

Figure 1. Chemical structure of molecule **AQ-1** and **AQ-2**.

Results and Discussion

Synthesis of Anthraquinone-Based Switches

The synthetic strategy used for the preparation of the target anthraquinone-based molecular switches **AQ-1** and **AQ-2** is based on an assembly of building blocks via Sonogashira cross-coupling reaction with commercially available 2,6-dibromo-9,10-anthraquinone **1** and the corresponding acetylenes as outlined in *Scheme 1*. For the preparation of **AQ-1** terminated with 4-pyridyl group, the corresponding 4-ethynylpyridine **2**, which is thermally and light unstable, was prepared in good yield according to a previously published procedure starting from commercially available 4-bromopyridine.[47] The freshly prepared derivative **2** was subsequently reacted with 2,6-dibromo-9,10-anthraquinone **1** using a palladium-catalyzed reaction in the dark and in a mixture of solvents due to the very low solubility of 2,6-dibromo-9,10-anthraquinone. After purification and recrystallization, the target molecule **AQ-1** was obtained in 72% yield. For the preparation of the second derivative **AQ-2**, the corresponding phenylacetylene compound **3** terminated with 2-(trimethylsilyl)ethylsulfanyl group was prepared in three reaction steps, starting first with protection of the thiol in 4-bromothiophenol and its subsequent Sonogashira reaction with ethynyltrimethylsilane followed by deprotection of the terminal TMS group according to previously published literature.[48,49] Thus prepared phenylacetylene derivative **3** was subsequently coupled with 2,6-dibromo-9,10-anthraquinone in a solvent mixture to afford the

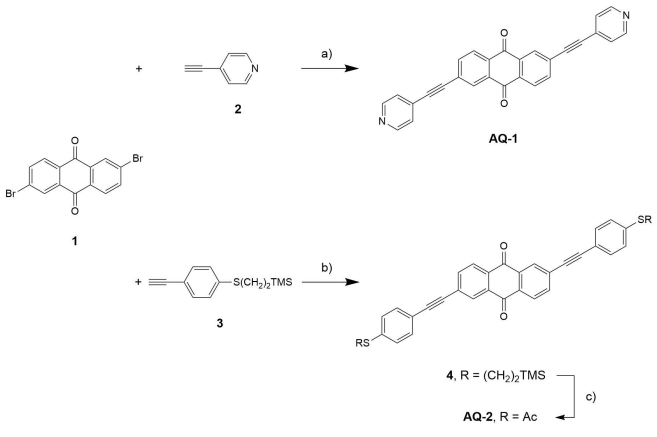

Scheme 1. Synthetic approach to anthraquinone-based switches **AQ-1** and **AQ-2**. Reaction conditions: a) $PdCl_2(PPh_3)_2$, CuI, THF, toluene, Et_3N, 85 °C, 72%; b) $PdCl_2(PPh_3)_2$, CuI, dioxane, toluene, Hünig base, 90 °C, 80%; c) AcCl, $AgBF_4$, $CHCl_3$, 69%.

title 2-(trimethylsilyl)ethylsulfanyl terminated anthraquinone **4** in 80% yield. The final transprotection of thiol was successfully performed using $AgBF_4$ and acetyl chloride (AcCl) to obtain the desired thioacetate derivative **AQ-2** in 69% yield. The acetyl serves as a labile thiol protecting group and can mildly and efficiently be cleaved prior to physical investigations or *in situ* upon binding to the gold surface.

STM Break Junction (STM BJ) Characterization

Figure 2 shows representative semilogarithmic conductance-distance curves for molecules **AQ-1** and **AQ-2**. They exhibit characteristic conductance plateaus indicating that the molecule bridged both gold electrodes to create a single molecule junction. This feature is missing in the absence of molecules in the junction (grey curve). Each plateau has a characteristic length Δz, which relates to the experimental MJ length z^{exp} through the equation $z^{exp} = \Delta z + 0.4$ nm. The correction factor 0.4 nm signifies the experimentally-obtained snap-back distance in the absence of molecule.[34]

Several hundreds of conductance-distance curves without any data selection were used to construct 1D conductance (*Figure 3*) and 2D conductance-distance (*Figure 4*) histograms. *Figure 3* displays the characteristic conductance peaks, which indicate the most probable conductances of STM BJ prepared gold-molecule-gold junctions. Two stable MJ configurations were observed for molecule **AQ-1**, whereas only one for **AQ-2**, respectively. The 2D conductance-distance histograms show two distinct plateaus with high G_H and low G_L conductance for molecule **AQ-1** and only one low conductance plateau for **AQ-2** which is consistent with *Figure 3*.

The low conductance plateaus in *Figure 4* were used to determine the most probable MJ length z^{exp} values via construction of the plateau length Δz histograms at constant $\log(G/G_0)$ values just below the experimental MJ conductance $\log(G_L/G_0)^{exp}$. The corresponding plateau length histograms are given in *Figure 5* together with the best Gaussian fit of the peak providing the most probable Δz value, which after the snap-back correction gives the experimental MJ length values z_L^{exp}. *Table 1* summarizes experimentally-obtained $\log(G_L/G_0)^{exp}$ and z_L^{exp} values for low conductance plateau configurations of both molecules. The G_H plateau feature for **AQ-1** was also analyzed and the experimentally-obtained value of $\log(G_H/G_0)^{exp}$ equals to -4.2 ± 0.4 at $z_H^{exp} = 1.1 \pm 0.1$ nm, respectively. The high conductance plateau length

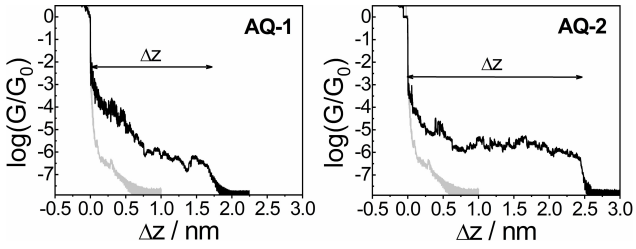

Figure 2. Representative conductance-distance curves for molecule **AQ-1** (left) and **AQ-2** (right). Double arrow indicates plateau length Δz. Grey curve shows tunneling current in mesitylene solvent in the absence of molecules.

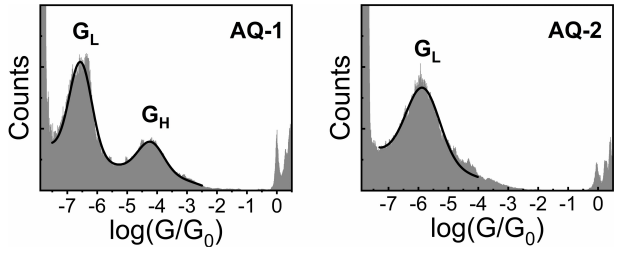

Figure 3. Experimental 1D logarithmic conductance histogram (counts vs $\log(G/G_0)$) for MJ of molecule **AQ-1** (left) and **AQ-2** (right). High and low conductance peak is labelled G_H and G_L, respectively.

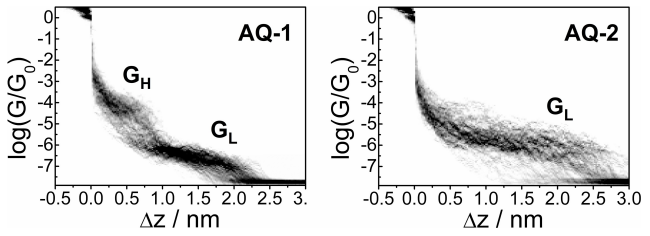

Figure 4. 2D semilogarithmic conductance-distance ($\log(G/G_0)$ vs Δz) histogram for MJ of molecule **AQ-1** (left) and **AQ-2** (right). High and low conductance plateau is labelled G_H and G_L, respectively.

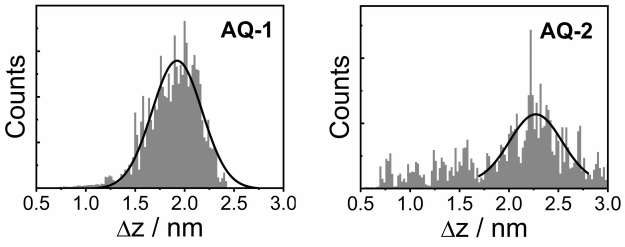

Figure 5. Plateau length histogram obtained at $\log(G/G_0) = -7.3$ for molecule **AQ-1** and at $\log(G/G_0) = -7.0$ for molecule **AQ-2**, respectively.

Table 1. Experimental and theoretical conductance and MJ length values.

MJ	log $(G_L/G_0)^{exp}$	z_L^{exp}/nm	log $(G_L/G_0)^{th}$	z_L^{th}/nm
AQ-1	-6.6 ± 0.4	2.3 ± 0.3	-6.3 ± 0.2	2.1
			-2.1 ± 0.1[a]	2.7[a]
AQ-2	-5.9 ± 0.6	2.7 ± 0.3	-8.1 ± 0.3[b]	2.5[b]
			-9.0 ± 0.5[c]	2.9[c]

[a] Deprotected **AQ-2** thiolate connected via sulfur atom. [b] **AQ-2** connected via sulfur atom. [c] **AQ-2** connected via oxygen atom.

histogram used for the determination of z_H^{exp} value is shown in *Section 2* of the *Supporting Information*.

Molecule **AQ-2** can be considered as a precursor for thiolates that can be formed *in-situ* via deprotection or upon **AQ-2** binding to the gold surface. We opted for the latter type of MJ formation excluding a deprotection agent, since the presence of triethylamine led to the aggregate formation and their precipitation onto the electrode surface.

Results in *Figures 3* to *5* provide evidence that phenylene thioacetate functional group leads to **AQ-2** junctions with predominantly one type of MJ configuration and the most probable conductance value $G_L = 0.1$ nS. In the case of 4-pyridyl anchors (**AQ-1** junctions) two configurations are possible with high conductance G_H equal to 4.9 nS and low conductance G_L equal to 20 pS. Considering only the retraction curves with a confirmed conductance plateau, then 64.8% of **AQ-1** junctions display both G_H and G_L configurations, 32.7% go directly to G_L configuration and only 2.5% junctions break after reaching the G_H configuration. So, almost all junctions (97.5%) reach the G_L configuration that corresponds to a fully extended molecule between the gold leads, see the experimental z_L^{exp} value in *Table 1*.

Junction formation probability for **AQ-1** devices is slightly higher (~96%) than for those containing **AQ-2** molecules (~89%), which is consistent with previously reported values for pyridyl- and thiol-type anchoring groups.[9,24,26] Thiol-terminated molecules displayed also higher conductance than pyridyl-terminated ones.[24,27]

DFT/NEGF Charge Transport Characterization

Theoretical MJ transmission function T(E) and conductance G^{th} values were calculated using the non-equilibrium Green's function formalism (NEGF) in combination with Density functional theory (DFT) at zero-bias approximation.[50] Theoretical conductance was calculated using Landauer formula $G^{th} = G_0 \times T(E_F)$, where G_0 is the conductance quantum and $T(E_F)$ is the transmission function at the Fermi level of the gold electrodes $E_F = -5.1 \pm 0.1$ eV. Additional computational details are provided in the *Experimental Section* and in our previous publications.[34,35,51]

Molecules **AQ-1** and **AQ-2** are prototypical cross-conjugated systems,[52] which are expected to display destructive quantum interference (QI). QI demonstrates itself as a sharp decrease (dip) in the transmission function. This feature was reproduced in our charge transport calculations as well, but as previously pointed out,[52] the conductance values calculated for MJs of this type of molecules are strongly sensitive to the position of Fermi level, which is difficult to calculate within the current DFT approach.[52]

Quantum chemical methodology reproduces the experimental conductance for MJs of **AQ-1** reasonably well, see *Table 1*, *Figure 6* and *Section 3* of the SI. Theoretical value for high conductance MJ configuration, which is consistent with the experimental log $(G_H/G_0)^{exp}$ is log $(G_H/G_0)^{th} = -4.0 \pm 0.1$. The corresponding theoretical MJ configuration (see *Figure S8*) indicates that the contact between **AQ-1** molecule and the gold electrode is mainly via the interaction between π electrons of the aromatic ring and the gold atoms. The contribution of lone electron pairs of either the nitrogen of the 4-pyridine anchor or of the carbonyl oxygens of the anthraquinone moiety is not excluded, but less likely. We remind the readers that G_H plateau is not observed for **AQ-2** molecular junctions, which contain the same anthraquinone moiety. Thus, the most probable scenario for the **AQ-1** junction evolution would be the sliding mechanism along the 4-pyridine anchor up to the point, when a stable G_L configuration is achieved due to a relatively strong Au–N interaction. As the distance between electrodes increases the electrons of the aromatic ring

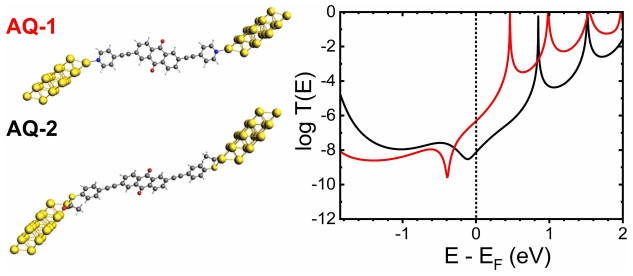

Figure 6. MJ configuration (left) and transmission function T(E) (right) for MJ of molecule **AQ-1** (red) via 4-pyridyl and **AQ-2** (black) via sulfur atom of phenylene thioacetate anchor.

decrease their contribution towards the charge transport and the second configuration employing Au–N bonding prevails. The theoretical value for the low conductance MJ configuration is log $(G_L/G_0)^{th} = -6.3 \pm 0.2$, which is in excellent agreement with the experimental measurements, see *Table 1*. Clearly, the **AQ-1** molecules form in their low conductance state fully extended junctions, see *Figure 6*.

The difficulty connected with computing the MJ conductance of **AQ-2** comes from the fact that more than one anchoring possibility can occur. Nevertheless, even though these calculations do not accurately reproduce the experimental conductance for MJ of **AQ-2**, they provide strong evidence that a direct contact between molecule and electrodes via thiolate bond is in operation, see *Table 1*, *Figure 6* and *Section 4* of the SI. DFT/NEGF computation of the MJ conductance for the **AQ-2** molecule after the complete thioacetate deprotection (no acetyl in the junction) provided log $(G_L/G_0)^{th}$ value of -2.1 ± 0.1 at $z_L^{th} = 2.7$ nm, which is much higher than that observed experimentally. Molecule **AQ-2** connected via oxygen atom from the acetyl groups has theoretical conductance $\log(G_L/G_0)^{th}$ equal to -9.0 ± 0.5, which is lower than the experimental value. In this case, the MJ length z_L^{th} of 2.9 nm is too long in comparison with the experiment. Thus, the most plausible MJ arrangement seems to be via sulfur atoms of the thioacetate anchor. Our DFT/NEGF calculations for **AQ-2** molecular junction indicate that real MJ configurations most likely include a combination of connections between **AQ-2** molecule and gold electrodes through sulfur which is either free of or still connected to the acetyl group.

Conclusions

Charge transport properties of **AQ-1** and **AQ-2** single molecule junctions have been studied using STM BJ measurements and quantum mechanical calculations in order to find the most suitable anchoring group for the switching purposes. **AQ-1** and **AQ-2** molecules contain identical anthraquinone center (switching element) and differ in the type of anchoring group (4-pyridyl versus *p*-phenylene thioacetate). Both molecules represent an OFF state of an ON/OFF conductance switch based on the anthracene-9,10-diol/anthraquinone redox couple. The reliable switching requires high junction formation probability and the lowest possible conductance for the OFF state. As the anthraquinone backbone represents the OFF state of such a switch the most suitable molecule should have both the highest junction formation probability as well as the lowest possible conductance. It has been shown that single molecule junctions anchored to the metallic electrodes by nitrogen atom of the pyridyl group have the higher junction formation probability compared to those anchored by sulfur atom of the thioacetate anchoring group. This represents an advantage. Such devices form **AQ-1** junctions in two different configurations whose conductance differ by several orders of magnitude (4.9 nS and 20 pS). However, the most stable configuration is the one with the conductance of 20 pS. Molecule **AQ-2** on the other hand forms junctions in one prevailing configuration with a corresponding conductance of 0.1 nS. Quantum chemical calculations revealed the existence of a destructive QI effect in both types of molecular junctions, which relates to the cross-conjugation pattern of the anthraquinone center. Based on these results, one can conclude that for switching purposes MJs of **AQ-1** molecules are better suited for *redox-active* switching due to their higher junction formation probability and lower conductance.

Experimental Section

General Experimental Details and Materials

All starting materials and reagents were purchased from commercial suppliers and used without further purification. Solvents utilized for crystallization, chromatography and extraction were used in technical grade. Anhydrous tetrahydrofuran, toluene and dichloromethane were taken from MBraun Solvent Purification System equipped with drying columns. Triethylamine and $CHCl_3$ were dried and distilled from CaH_2 under nitrogen atmosphere. TLC was performed on silica gel 60 F254 plates, spots were detected by fluorescence quenching under UV light at 254 nm and 366 nm. Column chromatography was performed on silica gel 60 (particle size 0.040–0.063 mm). Compounds **2**[47] and **3**[48,49] were prepared according to a published procedure. Chemical synthesis and characterization of all new molecules are given bellow. All compounds were purified by chromatography and fully characterized by means of conventional NMR, FTIR spectroscopy, mass spectrometry, as well as by elemental analysis.

All commercially available reagents for sample preparation and STM BJ measurements were used as received. This included 1,3,5-trimethylbenzene (mesity-

lene, 98% Sigma Aldrich), triethylamine (BioUltra, ≥ 99.5% Sigma Aldrich), tetrahydrofuran (THF anhydrous, 99.9% Sigma Aldrich), ethanol (absolute, p. a. Penta, Czech Republic), nitric acid (65% p. a. Lach-Ner, Czech Republic) and nitrogen gas (99.996% Messer). Ultrapure deionized water (minimum resistivity 18.2 MΩ·cm and TOC of 3 ppb), prepared in Milli-Q Integral 5 water purification system (Merck Millipore), was used for cleaning purposes.

Equipment and Measurements

NMR spectra were recorded on a Bruker Avance III 500 or Bruker Avance NEO 400 spectrometer at 25 °C in $CDCl_3$. ^{1}H-NMR (500 MHz, 400 MHz) spectra were referred to the solvent residual proton signal ($CDCl_3$, $\delta_H = 7.24$ ppm). ^{13}C NMR (126 MHz, 101 MHz) spectra with total decoupling of protons were referred to the solvent ($CDCl_3$, $\delta_C = 77.23$ ppm). For correct assignment of both ^{1}H and ^{13}C NMR spectra, ^{1}H–^{1}H COSY, ^{13}C DEPT-135, HSQC, HMBC experiments were performed. EI MS spectra were recorded with a Thermo Trace 1300-ISQ GC/MS instrument (samples were introduced directly using direct injection probes DIP, DEP) and m/z values are given along with their relative intensities (%) at an ionization voltage of 70 eV. IR spectra were recorded with a Nicolet iS50 FTIR spectrometer under ATR mode. Analytical samples were dried at 40–100 °C under reduced pressure ($\approx 10^{-2}$ mbar). Melting points were measured with a Büchi Melting point M-560 apparatus and are uncorrected. Elemental analyses were obtained with a Vario MicroCube CHNS analyzer. The values are expressed in mass percentage. The NMR spectra of previously unpublished molecules are given in the *Supporting Information*, along with the molecular structure and atom numbering used for the full assignments of signals in the NMR spectra.

Experimental Details and Synthetic Procedures

2,6-Bis(pyridin-4-ylethynyl)anthracene-9,10-dione (**AQ-1**)

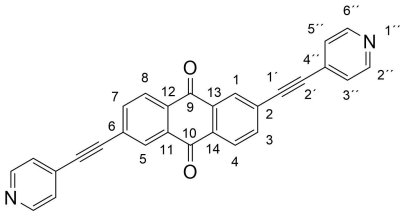

In an oven dried 100 ml Schlenk flask, 2,6-dibromo-9,10-anthraquinone (200 mg, 0.55 mmol) was suspended in the mixture of anhydrous THF (50 ml), toluene (20 ml), triethylamine (10 ml) and purged with argon for 10 min before addition of $PdCl_2(PPh_3)_2$ (60 mg, 86 μmol) and anhydrous CuI (33 mg, 173 μmol). Finally, 4-ethynylpyridine **2** (170 mg, 1.65 mmol, 3 eq) was added under argon and the dark brown suspension was heated at 85 °C for 16 h in dark (wrapped with aluminum foil) while the reaction progress was monitored by TLC in $CHCl_3$. After cooling down to room temperature, the suspension was diluted with $CHCl_3$ (100 ml), passed over a pad of silica gel (50 g) + Celite (10 g), washed with $CHCl_3$ (100 ml) and $CHCl_3$:CH_3OH (10:1, 150 ml). After evaporation of all volatiles, the crude product was absorbed on silica gel (1 g) and purified by column chromatography on silica gel (200 g) in the gradient of $CHCl_3$ to $CHCl_3$:CH_3OH (10:1) to afford the product as an orange powder. The title compound was finally purified via recrystallization from toluene (40 ml) to yield the pure anthraquinone derivative **AQ-1** (163 mg, 72%) as a light-yellow powder. $R_f = 0.44$ ($CHCl_3$:CH_3OH = 20:1); M.p. 348.2 °C (dec.); ^{1}H-NMR (500 MHz, $CDCl_3$) δ (ppm) = 8.66 (d, J = 6.9 Hz, 4H, $C^{2'',6''}H$), 8.46 (d, J = 1.4 Hz, 2H, $C^{1,5}H$), 8.33 (d, J = 8 Hz, 2H, $C^{4,8}H$), 7.93 (dd, J = 8.0, 1.3 Hz, 2H, $C^{3,7}H$), 7.42 (d, J = 4.6 Hz, 4H, $C^{3'',5''}H$); ^{13}C NMR (126 MHz, $CDCl_3$) δ (ppm) = 181.9 (CO), 150.2 ($C^{2'',6''}H$), 137.1 ($C^{3,7}H$), 133.7 ($C^{11,13}$), 133.0 ($C^{12,14}$), 131.0 ($C^{1,5}H$), 130.5 ($C^{4''}$), 128.8 ($C^{2,6}$), 127.9 ($C^{4,8}H$), 125.8 ($C^{3'',5''}H$), 92.0 ($-C^{1'}\equiv$), 91.4 ($\equiv C^{2'}-$); FTIR (ATR): $\tilde{\nu}$ (cm^{-1}) = 3062 (w, ν(CH)), 3038 (m, ν(CH)), 3016 (w), 1676 (s, ν(C=O), AQ), 1664 (m), 1590 (vs, ν(CC)), 1407 (m, ν(CC)), 1324 (s), 1303 (m), 1275 (s), 1246 (m), 1180 (w), 985 (m), 884 (m), 857 (w), 817 (s, δ(CH)), 739 (m), 708 (m), 580 (w), 549 (m); MS (EI, 70 eV) m/z (%): 411.2 (28), 410.1 (100, $[M]^+$), 382.1 (19), 354.2 (13), 325.1 (11), 205.2 (25), 150.1 (15), 149.1 (15), 137.0 (12), 136.0 (15), 124.0 (12); Anal. calc. for $C_{28}H_{14}N_2O_2$ (410.11): C 81.94, H 3.44, N 6.83, Found: C 81.63., H 3.56, N 6.69.

2,6-Bis{4-[2-(trimethylsilyl)ethylsulfanyl]phenylethynyl} anthracene-9,10-dione (**4**)

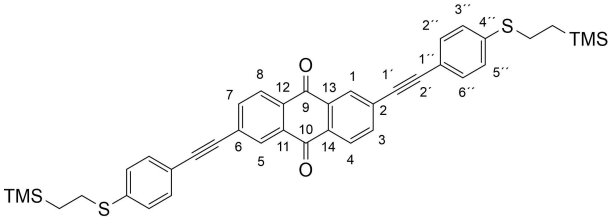

The brown suspension of 2,6-dibromo-9,10-anthraquinone (200 mg, 0.55 mmol) in anhydrous dioxane (40 mL), Hünig base (10 ml) and toluene (20 ml) in a

100 ml Schlenk flask was flushed with argon for about 10 min before addition of $PdCl_2(PPh_3)_2$ (60 mg, 86 μmol) and anhydrous CuI (33 mg, 173 μmol). Subsequently, 1-ethynyl-4-[2-(trimethylsilyl)ethylsulfanyl]benzene **3** (352 mg, 1.5 mmol) in anhydrous dioxane (10 ml) was added and the dark suspension was heated at 90 °C for 18 h while the reaction progress was monitored by TLC in the mixture of hexane:CH_2Cl_2 (1:1). After cooling down to room temperature, the greenish suspension was diluted with $CHCl_3$ (100 ml), passed over a pad of silica gel (40 g) + Celite (10 g), washed with $CHCl_3$ (100 ml), $CHCl_3$:CH_3OH (10:1, 100 ml) and hot toluene (100 ml). After evaporation of all volatiles, the crude product was absorbed on silica gel (1 g) and purified by column chromatography on silica gel (300 g) in the gradient of hexane:CH_2Cl_2 (5:1) to hexane:CH_2Cl_2 (1:1) to afford the product as an orange powder. The desired compound was finally purified via recrystallization from toluene (30 ml) to yield the pure compound **4** (295 mg, 80 %) as a pale-yellow powder. $R_f = 0.41$ (hexane:CH_2Cl_2 = 1:1); M.p. 236.5 °C; ^{1}H-NMR (400 MHz, $CDCl_3$) δ (ppm) = 8.40 (d, J = 1.6 Hz, 2H, $C^{1,5}$H), 8.28 (d, J = 8 Hz, 2H, $C^{4,8}$H), 7.87 (dd, J = 8.0, 1.6 Hz, 2H, $C^{3,7}$H), 7.46 (dd, J = 8.4, 1.7 Hz, 4H, $C^{2'',6''}$H), 7.42 (dd, J = 8.0, 1.7 Hz, 4H, $C^{3'',5''}$H), 2.94-3.10 (m, 4H, -SC$\underline{H_2}$), 0.91-0.98 (m, 4H, C$\underline{H_2}$Si−), 0.05 (s, 18H, TMS); ^{13}C NMR (101 MHz, $CDCl_3$) δ (ppm) = 182.2 (CO), 140.2 ($C^{4''}$), 136.6 ($C^{3,7}$H), 133.8 ($C^{11,13}$), 132.4 ($C^{2'',6''}$H), 132.3 ($C^{12,14}$), 130.4 ($C^{1,5}$H), 130.2 ($C^{2,6}$), 127.8 ($C^{3'',5''}$H), 127.7 ($C^{4,8}$H), 119.0 ($C^{1''}$), 94.8 (≡$C^{2'}$−), 88.6 (−$C^{1'}$≡), 28.9 (−S$\underline{C}H_2$), 16.8 ($\underline{C}H_2$Si−), −1.5 (CH_3, TMS); FTIR (ATR): $\tilde{\nu}$ (cm^{-1}) = 3067 (w, ν(CH)), 2949 (m, $\nu_{as}(CH_3)$), 2918 (w, $\nu_{as}(CH_2)$), 2891 (w, $\nu_s(CH_3, CH_2)$), 2204 (m, ν(C≡C)), 1668 (s, ν(C=O), AQ), 1582 (vs, ν(CC)), 1494 (m, ν(CC)), 1401 (w, ν(CC)), 1327 (m), 1303 (m), 1277 (s), 1245 (s, $\delta_s(CH_3)$, TMS), 1187 (w), 1166 (w), 1089 (m), 1011 (w), 985 (m), 882 (w), 857 (m) and 837 (m, $\delta_{as}(CH_3)$, TMS), 814 (s, δ(CH)), 742 (w), 731 (w), 709 (w); MS (EI, 70 eV) m/z (%): 673.2 (2), 672.2 (5, $[M]^+$), 645.2 (5), 644.1 (8), 629.1 (2), 616.1 (10), 125.1 (12), 101.1 (17), 85.1 (20), 73.0 (100), 57.1 (17), 44.0 (26); Anal. calc. for $C_{40}H_{40}O_2S_2Si_2$ (672.20): C 71.38, H 5.99, Found: C 71.57., H 6.12.

2,6-Bis[4-(acetylsulfanyl)phenylethynyl]anthracene-9,10-dione (**AQ-2**)

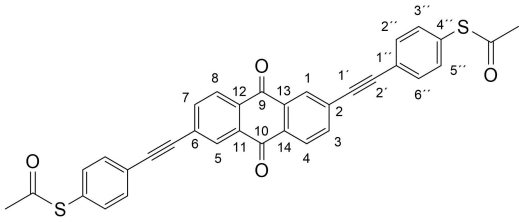

In an oven dried 60 ml Schlenk flask, the compound **4** (90 mg, 134 μmol, 1 eq) was dissolved in dry $CHCl_3$ (30 ml), cooled down to 0 °C and flushed with argon for about 10 min. Then, acetyl chloride (2 ml) was added, and the mixture was stirred for 5 min before $AgBF_4$ (104 mg, 536 mmol, 4 eq) was added under argon. The original dark red suspension dissolved and after about 20 min, white precipitate of AgCl was observed. A milky suspension was allowed to warm to room temperature and keep stirring for additional 8 h under argon. The reaction mixture was quenched with crashed ice (≈100 g) and diluted with $CHCl_3$ (70 ml). After extraction with $CHCl_3$ (3×80 ml), the combined organic layer was dried with $MgSO_4$. After filtration and evaporation of all volatiles at room temperature, the crude product was absorbed on silica gel (1 g) and purified by flash chromatography on silica gel (150 g) in the gradient of hexane:CH_2Cl_2 (1:2) to pure CH_2Cl_2. After drying, 52 mg (69 %) of the title compound **AQ-2** was isolated as a pale-yellow solid, which is very poorly soluble in all organic solvents, thus significantly influencing its characterization. The measured spectroscopic data are consistent with the previously reported literature.[52] $R_f = 0.45$ (CH_2Cl_2); ^{1}H-NMR (500 MHz, $CDCl_3$) δ (ppm) = 8.43 (d, J = 1.5 Hz, 2H, $C^{1,5}$H), 8.30 (d, J = 8 Hz, 2H, $C^{4,8}$H), 7.90 (dd, J = 8.0, 1.6 Hz, 2H, $C^{3,7}$H), 7.59 (d, J = 8.3 Hz, 4H, $C^{2'',6''}$H), 7.43 (d, J = 8.3 Hz, 4H, $C^{3'',5''}$H), 2.44 (s, 6H, CH_3, SAc); ^{13}C NMR (126 MHz, $CDCl_3$) δ (ppm) = 193.4 (CO, SAc), 182.1 (CO, AQ), 136.9 ($C^{3,7}$H), 134.5 ($C^{3'',5''}$H), 133.7 ($C^{11,13}$), 132.7 ($C^{2'',6''}$H), 132.6 ($C^{12,14}$), 130.6 ($C^{1,5}$H), 129.7 ($C^{2,6}$), 129.5 ($C^{4''}$), 127.8 ($C^{4,8}$H), 123.6 ($C^{1''}$), 93.8 (≡$C^{2'}$−), 89.7 (−$C^{1'}$≡), 30.6 (CH_3, SAc); FTIR (ATR): $\tilde{\nu}$ (cm^{-1}) = 3064 (w, ν(CH)), 2953 (m, $\nu_{as}(CH_3)$), 2921 (m, $\nu_{as}(CH_3)$), 2850 (m, $\nu_s(CH_3)$), 2218 (m, ν(C≡C)), 1702 (vs, ν(C=O), Ac), 1670 (vs, ν(C=O), AQ), 1589 (vs, ν(CC)), 1475 (w, ν(CC)), 1397 (w, ν(CC)), 1353 (w), 1324 (s), 1303 (m), 1276 (vs), 1245 (m), 1174 (w), 1120 (m), 1100 (m), 1089 (m), 1014 (w), 981 (m), 957 (m), 919 (w), 881 (w), 862 (w), 827 (s, δ(CH)), 741 (m), 711 (m), 663 (w), 617 (w), 602 (m), 579 (w), 542 (m), 450 (w); MS (EI, 70 eV) m/z (%): 556.1 (4, $[M]^+$), 514.1 (18), 472.1 (54), 85.0 (12), 83.0 (15), 44.0

(100), 43.0 (23), 28.0 (20); Anal. calc. for $C_{34}H_{20}O_4S_2$ (556.08): C 73.36, H 3.62, Found: C 73.61., H 3.45.

STM BJ Sample Preparation

Laboratory glassware, gold substrate, PTFE cells and sealing Kalrez O-rings (DuPont) were cleaned by boiling in a 25% nitric acid in ultrapure water and subsequently repeatedly boiled in ultrapure water and dried overnight at a temperature of 120 °C. After boiling in acid, the gold substrate was thoroughly rinsed with and stored in ultrapure water. The substrate was annealed with a propane butane flame and cooled in a nitrogen gas atmosphere just before the STM BJ measurement. Concentration of both molecules in STM BJ cell was 5×10^{-4} M (100 μL volume was utilized). Solution of **AQ-1** was prepared in pure mesitylene. Solution of **AQ-2** was prepared in 10% v/v THF in mesitylene to improve its solubility.

STM BJ Measurements

STM BJ measurements were performed using modified Agilent 5500 SPM microscope (Agilent Technologies, U.S.A.). Proper reference to its electronic modification is given elsewhere.[34,51] Briefly, STM BJ method is based on a repeated formation and breaking of the contact between two electrodes (STM tip and conducting substrate) in solution of studied compound while measuring current *i* flows through such junctions under the applied voltage difference between these electrodes, called bias voltage E_{bias}. Single molecule conductance G is obtained from statistical analyses of several hundreds of current-distance curves assuming that the conductance G follows the Ohm's law, *i.e.* $G = i/E_{bias}$. In this work, an electrochemically-etched gold wire (diameter 0.25 mm, 99,99%, Goodfellow, UK) was used as the STM tip and the gold plate (10 × 10 × 1 mm, 99.95%, Goodfellow, UK) was used as the substrate. The applied bias voltage was 0.13 V. The retraction rate in all experiments was 0.92 nm s^{-1}. All measured retraction curves were used to construct 1D conductance and 2D conductance-distance histograms using $\log(G/G_0)$ scale, where $G_0 = 77.5$ μS is the conductance quantum.

Computational Methods

Molecules **AQ-1** and **AQ-2** were geometrically-optimized in vacuum using B3LYP DFT functional with inclusion of D3 dispersion coefficient employing 6–31G(d,p) basis set.[34,35]

MJ was prepared by placing geometrically-optimized molecules in-vacuo between two Au_{18} clusters and optimizing the distance between the top gold atom of each Au_{18} cluster. The Au_{18} clusters were modelled using two layers of gold atoms corresponding to the Au(111) arrangement and having interatomic distances of 2.885 Å representing the bulk gold. The relativistic pseudopotential with relevant basis set LANL2DZ was used for Au_{18} cluster optimization.[53]

Molecule **AQ-2** was contacted to gold clusters either through the oxygen or sulfur atom of the acetyl-S group or through the sulfur atom directly in the absence of the acetyl group considering its cleavage. In the first case, the distance between top gold atoms of two gold clusters (oxygen atom contact) was systematically varied between 31.0 Å and 32.9 Å employing 0.1 Å step. In the second case, the distance between the top gold atoms of the clusters increased from 26.0 Å to 27.5 Å also in 0.1 Å step. In the third case, the electronic energy within a self-consistent field procedure converged very slowly. Therefore, only one MJ configuration was calculated with the distance of 29.9 Å between the top gold atoms of the gold clusters. All calculations in this section were performed using Gaussian 16, Revision C.01 quantum chemistry program.[54]

The geometrically-optimized MJ configuration corresponding to minimum on the potential energy surface was used for DFT/NEGF calculation of the transmission function T(E) as implemented in the ADF 2017 program, version 13.[55] Slater-type (double-ζ) DZ basis set was used for the Au atoms; Slater-type (double-ζ plus polarization function) DZP basis set for the N, O, H and C atoms. All calculations were performed with inclusion of the scalar relativistic effect within Zero Order Regular Approximation (ZORA) approach. The wide-band limit approximation (WBL) was used for DFT/NEGF transmission function calculations employing parameter $\Gamma = 0.5$ a.u., B3LYP functional and the frozen-core approximation of Slater basis sets.

Supporting Information

NMR spectra of all new compounds; plateau length analysis for high conductance MJ configuration of **AQ-1**; DFT/NEGF results for high conductance MJ configuration of **AQ-1**; DFT/NEGF results for different MJ configurations of **AQ-2**.

Author Contribution Statement

M. H. designed the experiments, analyzed data and wrote the paper with contributions from all authors. *F. V.* performed the STM-BJ measurements, analyzed data and assisted in manuscript editing. *M. V.* synthesized and characterized all molecules, *J. G.* wrote the program for data analysis, *J. Š.* conducted quantum chemical calculations and *G. M.* contributed to the design and development of STM BJ methodology.

Acknowledgements

This work was supported by the J. Heyrovský Institute of Physical Chemistry of the Czech Academy of Sciences (RVO: 61388955), Czech Science Foundation (21-13458S), and Mobility Plus Projects of the Czech Academy of Sciences (MTA-24-08). M. H. and J. Š. acknowledge the assistance provided by the Advanced Multiscale Materials for Key Enabling Technologies project, supported by the Ministry of Education, Youth, and Sports of the Czech Republic. Project No. CZ.02.01.01/00/22_008/0004558, Co-funded by the European Union. Financial assistance of the National Research, Development and Innovation Office through the projects OTKA–K-143169 and OTKA-FK-142622 is acknowledged. M. V. gratefully acknowledges funding by the Helmholtz Association via the program Materials Systems Engineering (MSE). Open Access publishing facilitated by Ustav fyzikalni chemie J Heyrovskeho Akademie ved Ceske republiky, as part of the Wiley - CzechELib agreement.

Data Availability Statement

The data that support the findings of this study are available from the corresponding author upon reasonable request.

References

[1] D. Xiang, X. Wang, Ch. Jia, T. Lee, X. Guo, 'Molecular-Scale Electronics: From Concept to Function', *Chem. Rev.* **2016**, *116*, 4318–4440.
[2] Z. Liu, S. Ren, X. Guo, 'Switching Effects in Molecular Electronic Devices', *Top. Curr. Chem.* **2017**, *375*, 56.
[3] T. Sendler, K. Luka-Guth, M. Wieser, Lokamani, J. Wolf, M. Helm, S. Gemming, J. Kerbusch, E. Scheer, T. Huhn, A. Erbe, 'Light-Induced Switching of Tunable Single-Molecule Junctions', *Adv. Sci.* **2015**, *2*, 1500017.
[4] G. Ke, Ch. Duan, F. Huang, X. Guo, 'Electrical and spin switches in single-molecule junctions', *InfoMat.* **2020**, *2*, 92–112.
[5] C. Tang, M. Shiri, H. Zhang, R. T. Ayinla, K. Wang, 'Light-Driven Charge Transport and Optical Sensing in Molecular Junctions', *Nanomaterials* **2022**, *12*, 698.
[6] N. Darwish, A. C. Aragonès, T. Darwish, S, Ciampi, I. Díez-Pérez, 'Multi-Responsive Photo- and Chemo-Electrical Single-Molecule Switches', *Nano Lett.* **2014**, *14*, 7064–7070.
[7] X. Liu, X. Li, S. Sangtarash, H. Sadeghi, S. Decurtins, R. Häner, W. Hong, C. J. Lambert, S.-X. Liu, 'Probing Lewis acid-base interactions in single-molecule junctions', *Nanoscale* **2018**, *10*, 18131–18134.
[8] S. Guo, J. M. Artés, I. Díez-Pérez, 'Electrochemically-gated single-molecule electrical devices', *Electrochim. Acta* **2013**, *110*, 741–753.
[9] C. Huang, A. V. Rudnev, W. Hong, T. Wandlowski, 'Break junction under electrochemical gating: testbed for single-molecule electronics', *Chem. Soc. Rev.* **2015**, *44*, 889–901.
[10] R. J. Nichols, S. J. Higgins, 'Single Molecule Nanoelectrochemistry in Electrical Junctions', *Acc. Chem. Res.* **2016**, *49*, 2640–2648.
[11] M. Hromadová, F. Vavrek, 'Electrochemical electron transfer and its relation to charge transport in single molecule junctions', *Curr. Opin. Electrochem.* **2020**, *19*, 63–70.
[12] H. M. Osorio, S. Catarelli, P. Cea, J. B. G. Gluyas, F. Hartl, S. J. Higgins, E. Leary, P. J. Low, S. Martín, R. J. Nichols, J. Tory, J. Ulstrup, A. Vezzoli, D. C. Milan, Q. Zeng, 'Electrochemical Single-Molecule Transistors with Optimized Gate Coupling', *J. Am. Chem. Soc.* **2015**, *137*, 14319–14328.
[13] S. Naghibi, S. Sangtarash, V. J. Kumar, J.-Z. Wu, M. M. Judd, X. Qiao, E. Gorenskaia, S. J. Higgins, N. Cox, R. J. Nichols, H. Sadeghi, P. J. Low, A. Vezzoli, 'Redox-Addressable Single-Molecule Junctions Incorporating a Persistent Organic Radical', *Angew. Chem. Int. Ed.* **2022**, *61*, e202116985.
[14] J. Li, S. Pudar, H. Yu, S. Li, J. S. Moore, J. Rodríguez-López, N. E. Jackson, C. M. Schroeder, 'Reversible Switching of Molecular Conductance in Viologens is Controlled by the Electrochemical Environment', *J. Phys. Chem. C* **2021**, *125*, 21862–21872.
[15] X. Xu, Ch. Gao, R. Emusani, Ch. Jia, D. Xiang, 'Toward Practical Single-Molecule/Atom Switches', *Adv. Sci.* **2024**, *11*, 2400877.
[16] D. Jago, Ch. Liu, A. H. S. Daaoub, E. Gaschk, M. C. Walkey, T. Pulbrook, X. Qiao, A. N. Sobolev, S. A. Moggach, D. Costa-Milan, S. J. Higgins, M. J. Piggott, H. Sadeghi, R. J. Nichols, S. Sangtarash, A. Vezzoli, G. A. Koutsantonis, 'An Orthogonal Conductance Pathway in Spiropyrans for Well-Defined Electrosteric Switching Single-Molecule Junctions', *Small* **2024**, *20*, 2306334.
[17] M. L. Perrin, E. Burzurí, H. S. J. van der Zant, 'Single-molecule transistors', *Chem. Soc. Rev.* **2015**, *44*, 902–919.
[18] H. B. Li, B. E. Tebikachew, C. Wiberg, K. Moth-Poulsen, J. Hihath, 'A Memristive Element Based on an Electrically Controlled Single-Molecule Reaction', *Angew. Chem. Int. Ed.* **2020**, *59*, 11641–11646.
[19] Y. Guo, Ch. Yang, S. Zhou, Z. Liu, X. Guo, 'A Single-Molecule Memristor based on an Electric-Field-Driven Dynamical Structure Reconfiguration', *Adv. Mater.* **2022**, *34*, 2204827.
[20] F. Chen, X. Li, J. Hihath, Z. Huang, N. Tao, 'Effect of Anchoring Groups on Single-Molecule Conductance: Com-

parative Study of Thiol-, Amine-, and Carboxylic-Acid-Terminated Molecules', *J. Am. Chem. Soc.* **2006**, *128*, 15874–15881.
[21] L. A. Zotti, T. Kirchner, J. C. Cuevas, F. Pauly, T. Huhn, E. Scheer, A. Erbe, 'Revealing the Role of Anchoring Groups in the Electrical Conduction Through Single-Molecule Junctions', *Small* **2010**, *6*, 1529–1535.
[22] E. Lörtscher, C. J. Cho, M. Mayor, M. Tschudy, C. Rettner, H. Riel, 'Influence of the Anchor Group on Charge Transport through Single-Molecule Junctions', *ChemPhysChem* **2011**, *12*, 1677–1682.
[23] J. R. Widawsky, P. Darancet, J. B. Neaton, L. Venkataraman, 'Simultaneous Determination of Conductance and Thermopower of Single Molecule Junctions', *Nano Lett.* **2012**, *12*, 354–358.
[24] W. Hong, D. Z. Manrique, P. Moreno-García, M. Gulcur, A. Mishchenko, C. J. Lambert, M. R. Bryce, T. Wandlowski, 'Single Molecular Conductance of Tolanes: Experimental and Theoretical Study on the Junction Evolution Dependent on the Anchoring Group', *J. Am. Chem. Soc.* **2012**, *134*, 2292–2304.
[25] Z. Li, M. Smeu, M. A. Ratner, E. Borguet, 'Effect of Anchoring Groups on Single Molecule Charge Transport through Porphyrins', *J. Phys. Chem. C* **2013**, *117*, 14890–14898.
[26] V. Obersteiner, D. A. Egger, E. Zojer, 'Impact of Anchoring Groups on Ballistic Transport: Single Molecule vs Monolayer Junctions', *J. Phys. Chem. C* **2015**, *119*, 21198–21208.
[27] E. Leary, A. La Rosa, M. T. González, G. Rubio-Bollinger, N. Agraït, N. Martin, 'Incorporating Single Molecules into Electrical Circuits. The Role of the Chemical Anchoring Group', *Chem. Soc. Rev.* **2015**, *44*, 920–942.
[28] S. R. Akbarabadi, M. M. Asl, 'Anchoring Groups Determine Conductance, Thermopower and Thermoelectric Figure of Merit of an Organic Molecular Junction', *Front. Phys.* **2021**, *9*, 727325.
[29] A. Daaoub, J. M. F. Morris, V. A. Béland, P. Demay-Drouhard, A. Hussein, S. J. Higgins, H. Sadeghi, R. J. Nichols, A. Vezzoli, T. Baumgartner, S. Sangtarash, 'Not So Innocent After All: Interfacial Chemistry Determines Charge-Transport Efficiency in Single-Molecule Junctions', *Angew. Chem. Int. Ed.* **2023**, *62*, e202302150.
[30] X. Wei, J. Wang, X. Chang, S. He, P. Duan, Ch. Jia, X. Guo, 'Interfacial Stereoelectronic Effect Induced by Anchoring Orientation', *Nano Lett.* **2024**, *24*, 9399–9405.
[31] B. Lawson, H. E. Skipper, M. Kamenetska, 'Phenol is a pH-activated linker to gold: a single molecule conductance study', *Nanoscale* **2024**, *16*, 2022–2029.
[32] Y. Li, Z. Zhang, R. Wang, A. Tang, Ch. Ma, Ch. Lian, H. Tian, H. Li, 'Suppressing the Conductance of Single-Molecule Junctions Fabricated by sp^2 C–H Bond Metalation', *ACS Appl. Mater. Interfaces* **2024**, *16*, 15426–15434.
[33] Z. Hu, Y. Wang, L. Liang, M. Wang, B. Xiao, Y. Li, 'A new anchoring group to fabricate single-molecule junctions: diphenyl sulfide', *J. Mater. Chem. C* **2024**, *12*, 854–858.
[34] J. Šebera, V. Kolivoška, M. Valášek, J. Gasior, R. Sokolová, G. Mészáros, W. Hong, M. Mayor, M. Hromadová, 'Tuning charge transport properties of asymmetric molecular junctions', *J. Phys. Chem. C* **2017**, *121*, 12885–12894.
[35] V. Kolivoška, J. Šebera, T. Sebechlebská, M. Lindner, J. Gasior, G. Mészáros, M. Mayor, M. Valášek, M. Hromadová, 'Probabilistic mapping of single molecule junction configurations as a tool to achieve the desired geometry of asymmetric tripodal molecules', *Chem. Commun.* **2019**, *55*, 3351–3354.
[36] J. Šebera, M. Lindner, J. Gasior, G. Mészáros, O. Fuhr, M. Mayor, M. Valášek, V. Kolivoška, M. Hromadová, 'Tuning the contact conductance of anchoring groups in single molecule junctions by molecular design', *Nanoscale* **2019**, *11*, 12959–12964.
[37] T. Ohto, A. Tashiro, T. Seo, N. Kawaguchi, Y. Numai, J. Tokumoto, S. Yamaguchi, R. Yamada, H. Tada, Y. Aso, Y. Ie, 'Single-Molecule Conductance of a π-Hybridized Tripodal Anchor while Maintaining Electronic Communication', *Small* **2021**, *17*, 2006709.
[38] J. S. Ward, A. Vezzoli, Ch. Wells, S. Bailey, S. P. Jarvis, C. J. Lambert, C. Robertson, R. J. Nichols, S. J. Higgins, 'A Systematic Study of Methyl Carbodithioate Esters as Effective Gold Contact Groups for Single-Molecule Electronics', *Angew. Chem. Int. Ed.* **2024**, *63*, e202403577.
[39] M. Valášek, M. Lindner, M. Mayor, 'Rigid multipodal platforms for metal surfaces', *Beilstein J. Nanotechnol.* **2016**, *7*, 374–405.
[40] M. Valášek, M. Mayor, 'Spatial and Lateral Control of Functionality by Rigid Molecular Platforms', *Chem. Eur. J.* **2017**, *23*, 13538–13548.
[41] S. Li, Y. Jiang, Y. Wang, D. Lin, H. Pan, Y. Wang, S. Sanvitod, S. Hou, 'Oxazine: an anchoring group serving as functional kernels to construct single-molecule switches', *J. Mater. Chem. C* **2024**, *12*, 2194–2202.
[42] L. Ornago, J. Kamer, M. El Abbassi, F. C. Grozema, H. S. J. van der Zant, 'Switching in Nanoscale Molecular Junctions due to Contact Reconfiguration', *J. Phys. Chem. C* **2022**, *126*, 19843–19848.
[43] S. Ghasemi, L. Ornago, Z. Liasi, M. B. Johansen, T. J. von Buchwald, A. E. Hillers-Bendtsen, S. van der Poel, H. Hölzel, Z. H. Wang, F. M. A. Noa, L. Öhrström, K. V. Mikkelsen, H. S. J. van der Zant, S. Lara-Avila, K. Moth-Poulsen, 'Exploring the impact of select anchor groups for norbornadiene/quadricyclane single-molecule switches', *J. Mater. Chem. C* **2023**, *11*, 15412–15418.
[44] E. H. van Dijk, D. J. T. Myles, M. H. van der Veen, J. C. Hummelen, 'Synthesis and Properties of an Anthraquinone-Based Redox Switch for Molecular Electronics', *Org. Lett.* **2006**, *8*, 2333–2336.
[45] M. Baghernejad, X. Zhao, K. B. Ørnsø, M. Füeg, P. Moreno-García, A. V. Rudnev, V. Kaliginedi, S. Vesztergom, C. Huang, W. Hong, P. Broekmann, T. Wandlowski, K. S. Thygesen, M. R. Bryce, 'Electrochemical Control of Single-Molecule Conductance by Fermi-Level Tuning and Conjugation Switching', *J. Am. Chem. Soc.* **2014**, *136*, 17922–17925.
[46] M. Carlotti, S. Soni, X. Qiu, E. Sauter, M. Zharnikov, R. C. Chiechi, 'Systematic experimental study of quantum interference effects in anthraquinoid molecular wires', *Nanoscale Adv.* **2019**, *1*, 2018–2028.
[47] S. Grunder, R. Huber, V. Horhoiu, M. T. González, C. Schönenberger, M. Calame, M. Mayor, 'New Cruciform Structures: Toward Coordination Induced Single Molecule Switches', *J. Org. Chem.* **2007**, *72*, 8337–8344.
[48] V. Kolivoška, M. Mohos, I. V. Pobelov, S. Rohrbach, K. Yoshida, W. J. Hong, Y. C. Fu, P. Moreno-García, G. Mészáros, P. Broekmann, M. Hromadová, R. Sokolová, M. Valášek, T. Wandlowski, 'Electrochemical Control of a Non-

Covalent Binding between Ferrocene and Beta-Cyclodextrin', *Chem. Commun.* **2014**, *50*, 11757–11759.
[49] M. A. Karimi, S. G. Bahoosh, M. Valášek, M. Bürkle, M. Mayor, F. Pauly, E. Scheer, 'Identification of the Current Path for a Conductive Molecular Wire on a Tripodal Platform', *Nanoscale* **2016**, *8*, 10582–10590.
[50] S. Datta, 'Nanoscale device modeling: the Green's function method', *Superlattices Microstruct.* **2000**, *28*, 253–278.
[51] Š. Nováková Lachmanová, V. Kolivoška, J. Šebera, J. Gasior, G. Mészáros, G. Dupeyre, P. P. Lainé, M. Hromadová, 'Environmental Control of Single-Molecule Junction Evolution and Conductance: A Case Study of Expanded Pyridinium Wiring', *Angew. Chem. Int. Ed.* **2021**, *60*, 4732–4739.
[52] H. Valkenier, C. M. Guédon, T. Markussen, K. S. Thygesen, S. J. van der Molen, J. C. Hummelen, 'Cross-Conjugation and Quantum Interference: A General Correlation?', *Phys. Chem. Chem. Phys.* **2014**, *16*, 653–662.
[53] P. J. Hay, W. R. Wadt, 'Ab-initio Effective Core Potentials for Molecular Calculations Potentials for K to Au Including the Outermost Core Orbitals', *J. Chem. Phys.* **1985**, *82*, 299–310.
[54] M. J. Frisch, G. W. Trucks, H. B. Schlegel, G. E. Scuseria, M. A. Robb, J. R. Cheeseman, G. Scalmani, V. Barone, G. A. Petersson, H. Nakatsuji, X. Li, M. Caricato, A. V. Marenich, J. Bloino, B. G. Janesko, R. Gomperts, B. Mennucci, H. P. Hratchian, J. V. Ortiz, A. F. Izmaylov, J. L. Sonnenberg, D. Williams-Young, F. Ding, F. Lipparini, F. Egidi, J. Goings, B. Peng, A. Petrone, T. Henderson, D. Ranasinghe, V. G. Zakrzewski, J. Gao, N. Rega, G. Zheng, W. Liang, M. Hada, M. Ehara, K. Toyota, R. Fukuda, J. Hasegawa, M. Ishida, T. Nakajima, Y. Honda, O. Kitao, H. Nakai, T. Vreven, K. Throssell, J. A. Montgomery, Jr., J. E. Peralta, F. Ogliaro, M. J. Bearpark, J. J. Heyd, E. N. Brothers, K. N. Kudin, V. N. Staroverov, T. A. Keith, R. Kobayashi, J. Normand, K. Raghavachari, A. P. Rendell, J. C. Burant, S. S. Iyengar, J. Tomasi, M. Cossi, J. M. Millam, M. Klene, C. Adamo, R. Cammi, J. W. Ochterski, R. L. Martin, K. Morokuma, O. Farkas, J. B. Foresman, D. J. Fox, Gaussian, Inc., Wallingford CT, **2019**.
[55] G. T. Te Velde, F. M. Bickelhaupt, E. J. Baerends, C. Fonseca Guerra, S. J. A. van Gisbergen, J. G. Snijders, T. Ziegler, 'Chemistry with ADF', *J. Comput. Chem.* **2001**, *22*, 931–967.

Received October 11, 2024
Accepted December 18, 2024

